



Evaluation of orange peel-derived activated carbons for treatment of dye-contaminated wastewater tailings

John Kwame Bediako^{1,2} · Shuo Lin¹ · Amit Kumar Sarkar¹ · Yufeng Zhao¹ · Jong-Won Choi¹ · Myung-Hee Song¹ · Chul-Woong Cho³ · Yeoung-Sang Yun¹

Received: 12 August 2019 / Accepted: 11 November 2019 / Published online: 9 December 2019
© Springer-Verlag GmbH Germany, part of Springer Nature 2019

Abstract

Dyes are colored compounds which are visible even at trace concentrations. Due to their recalcitrance and esthetic persistence, certain methods are unable to effectively eliminate them. So far, adsorptive treatment using activated carbons (ACs) is one of the most successful methods. In this study, we have employed orange peel (OP) as a cost-effective alternative to the expensive coal- and coir-based precursors to synthesize ACs for cationic methylene blue (MB) and anionic methyl orange (MO) dye adsorption. The pre-carbonized OP was activated via H₂SO₄, NaOH, KOH, ZnCl₂, and H₃PO₄ to study the effects of activation reagents on dye removal efficiencies and mechanisms. Among several isotherm models employed to fit the adsorption data, the Langmuir and Sips models sufficiently estimated the maximum equilibrium uptakes close to the experimental values of 1012.10 ± 29.13, 339.82 ± 6.98, and 382.15 ± 8.62 mg/g, for ZnCl₂-AC (MO), ZnCl₂-AC (MB), and KOH-AC (MB), respectively. The adsorption mechanisms were suggested to involve electrostatic binding, pi–pi interactions, hydrogen bonding, and electron donor–acceptor reactions. Consequently, more than 99% removal efficiency was achieved from a laboratory organic wastewater sample bearing ~ 35 mg/L of MB. The results thus suggest that the synthesized ACs from agricultural waste have the tendencies to be applied to real dye wastewater treatment.

Keywords Activated carbon · Characterization · Methylene blue · Methyl orange · Wastewater · Adsorption

Introduction

Dyes including methylene blue (MB) and methyl orange (MO) are high-intensity colored compounds with pronounced visibilities even at very low concentrations, which make them undesirable when present in effluents (Adegoke and Bello 2015; Vijayaraghavan and Yun 2007; Kelm et al. 2019).

Most industries, especially the textile, lithography, coating, pulp mill, and cosmetic industries, use dyes and pigments to color a wide range of products. It is estimated that an average of over 700,000 tons of more than 100,000 different kinds of commercially available dyes are produced on yearly basis (Li et al. 2013). The wastewaters discharged from these industries are thus laden with dyes and pigments which range between 5 and 1500 mg/L mean concentrations and tend to contaminate any water bodies that they come into contact with (Kim et al. 2015; Li et al. 2013).

Dye contamination of water resources has both esthetic and health effects as it may affect the photosynthetic activities of aquatic living things and cause cancer in most biological species including human beings (Adegoke and Bello 2015; Ngulube et al. 2017). This is because some dyes and their degraded products or intermediaries are not easily biodegradable. The removal of dyes from contaminated effluents is thus a major environmental concern that requires utmost attention. However, the decolorization of dye-contaminated effluents is problematic due to the difficulty in treating such wastewaters by some conventional treatment methods (Adegoke and Bello 2015; Vargas et al.

Responsible editor: Tito Roberto Cadaval Jr

✉ Chul-Woong Cho
choicejoe@jnu.ac.kr

✉ Yeoung-Sang Yun
ysyun@jbnu.ac.kr

¹ Division of Semiconductor and Chemical Engineering, Chonbuk National University, Jeonju, Jeonbuk 561-756, Republic of Korea

² Hongik University Research Institute of Science and Technology (HiRIST), Seoul, Republic of Korea

³ Department of Bioenergy Science and Technology, Chonnam National University, Gwangju, Republic of Korea

2011). The most commonly used treatment methods for dye wastewaters include biological oxidation and chemical precipitation techniques, which are expensive and require high concentrations of dyes for effective treatment. Adsorptive treatment has been identified as one of the best alternatives owing to its simplicity, low-cost, environmental benignity, and the ability to function effectively even at very low dye concentrations (Li et al. 2013; Vargas et al. 2011). Moreover, several classes of adsorbents including agricultural, microbial, synthetic polymer, carbon, clay, and zeolite-based adsorbents are available to choose from (Kim et al. 2015; Li et al. 2013; Sarkar et al. 2016; Vijayaraghavan and Yun 2007).

Adsorption using activated carbons (ACs) is one of the most widely known options; however, a major issue confronting its patronage is the high costs of commercial ACs which are usually sourced from coal, coir, and petroleum residues (Girods et al. 2009; Tan et al. 2008; Yagsi 2004; Yahya et al. 2015). Recent studies have suggested the use of agro-waste-derived ACs as cheaper alternatives. This proposal has received considerable acceptance owing to the ready availability and abundance of agro-waste precursors such as fruit peels, shells, nuts, and seeds (Vargas et al. 2011; Yahya et al. 2015). However, physicochemical characterizations providing sufficient insights into the biomass conversion processes and dye adsorption mechanisms have been seldom discussed in details. Moreover, most of the reported studies were limited to evaluating simulated solutions, leaving a wide gap between idealization and actualization. Understating the mechanisms involved in the biomass conversion and dye binding processes, coupled with full knowledge of the adsorption conditions, is believed to aid practical applications of adsorbents. Adegoke and Bello in their recent review of dye sequestration using agro-wastes as adsorbents emphasized that characterization of the adsorbents, adsorption conditions, and uptake mechanisms are highly desirable to design and carry out pilot-scale operations in order to study and check their feasibility at industrial level (Adegoke and Bello 2015). They also suggested that the low-cost alternative agro-waste adsorbents should be investigated using dye effluents from industries for their actual efficiency to be realized.

Fruits are agricultural crops grown and consumed all over the world, especially in the tropical and subtropical regions, where they are consumed as fresh (cut) fruits or food complements in desserts, salads, gelatins, fruit cocktails, jam, and juice combinations (Armando et al. 2001; Foo and Hameed 2012). The global annual productions of orange and banana, for example, are estimated by the Food and Agriculture Organization (FAO) at approximately 64 and 95.6 million metric tons, respectively (Foo and Hameed 2012; Spreen 2010). The peels of these fruits occupy nearly half of the total fruit weights. However, a lot of these wastes are indiscriminately disposed of unprocessed, and only few recycling or reuse attempts are made (Albarelli et al. 2011; González-Montelongo et al. 2010).

Therefore, it is important to consider reprocessing and reutilizing the fruit peels in other to add values to them and reduce their environmental effects (Foo and Hameed 2012). One of such recycling options is to employ them as precursor materials for the production of ACs for water treatment applications such as dye wastewater treatment.

A number of studies had already demonstrated the use of raw, carbonized, and activated agro-derived biomass for water decontamination, including dye adsorption. For example, cotton stalk was evaluated under three conditions, i.e., without treatment, H_2SO_4 - and H_3PO_4 -treatments, which saw the acid-treated samples exhibit adsorption affinities for MB (Deng et al. 2011). Moreover, coconut coir carbon activated with $ZnCl_2$ (Sharma et al. 2010), marine algae carbon activated with H_3PO_4 (Salima et al. 2013), and flamboyant pod carbon activated with NaOH (Vargas et al. 2011) showed improved adsorptions of MB, malachite green, and safranin O. Just recently, a nitrogen-doped activated mesoporous carbon aerogel prepared from chitosan was evaluated for MO adsorption from aqueous solution (Jiang et al. 2019). As stated earlier, despite the many reports, there still remain some knowledge gaps regarding the factors driving the activation processes for producing high-performing activated carbons, the effects of activation reagents, and mechanisms involved in the binding of target pollutants. In addition, only few studies have adequately demonstrated practical application potentials of the prepared activated carbons (Yagub et al. 2014; Pessôa et al. 2019). Thus, in this study, we have selected orange peel (OP) as a representative agro-waste precursor, along with five different kinds of activation agents, viz. H_2SO_4 , NaOH, KOH, $ZnCl_2$, and H_3PO_4 . The different activation agents were employed in order to test their effects on MB and MO adsorption capacities of the synthesized ACs. Moreover, several instrumental characterizations including FE-SEM, FTIR, XRD, and XPS were conducted to study the biomass conversion and dye adsorption mechanisms. For practical exploration, the synthesized ACs were eventually evaluated for adsorption of actual laboratory MB dye-containing organic wastewater, and the dye removal characteristics were thoroughly studied.

Materials and methods

Materials and reagents

The MB dye (CAS 7220-79-3; $C_{16}H_{18}ClN_3S \cdot 3H_2O$; M_w 373.9 g/mol; mp 190 °C), MO dye (CAS 547-58-0; $C_{14}H_{14}N_3NaO_3S$; M_w 327.33 g/mol; mp > 300 °C), $ZnCl_2$, and H_3PO_4 were purchased from Sigma-Aldrich Korea Ltd. (Yongin, South Korea). The KOH, NaOH, H_2SO_4 , and HCl were obtained from Daejung Chemicals and Metals Co., Ltd. (Gyeonggi-do, South Korea). The sun-dried fruit peel precursor, OP, was secured from Ghana and stored in an oven dryer

at 70 °C to maintain constant weight until use. Double distilled water (DW) was used throughout the study for washing and dilution and was obtained from a Direct-Q UV Millipore dispenser, Merck Millipore.

Synthesis of ACs

The OP biomass was washed with DW to wipe off adhering particles, and subsequently dried in an oven (Vision Scientific Co., Ltd.). It was then pulverized into coarse granules using a Philips blender (Allan Technology (Huizhou) Co., Ltd., China) and sieved through two layers of meshes, viz. 2 mm and 0.35 mm size meshes (standard testing sieves, Chung Gye Sang Gong SA., Seoul, South Korea). Those particles that passed through the 2-mm mesh but retained on the 0.35-mm mesh were selected and used for the synthesis of the ACs. About 6 g of the biomass was weighed into five crucibles and pre-carbonized in an automated furnace at 400 °C for 1 h under continuous N₂ flow. To evaluate the effects of different activation agents, the pre-carbonized precursors were impregnated with KOH, NaOH, H₂SO₄, H₃PO₄, and ZnCl₂ at fixed ratios of 2:1 (precursor: reagent) for 3 h. After that, the impregnated samples were filtered and dried in an oven dryer for ~24 h. The dried samples were placed back into the furnace for activation at 800 °C for 1 h under N₂ atmosphere. Consequently, the ACs were rinsed with DW, oven-dried for 24 h, and labeled according to the respective activation agents.

Characterization

The physicochemical characteristics of the ACs were examined via instrumental characterization. The surface morphologies were viewed on a field emission scanning electron microscope, FE-SEM (SUPRA 40VP, Carl Zeiss, Germany). N₂ adsorption isotherm and pore size distribution measurements were performed on a BELSORP-max BET equipment at 77 K. Crystallinity studies were conducted using an XRD (multipurpose high-performance X-ray diffractometer, X'pert Powder, PANalytical, the Netherlands) with a Cu-K α radiation source. In addition, functional groups analyses were performed with a Fourier transforms infrared spectrometer (PerkinElmer spectrophotometer: Spectrum GX, FTIR System) by employing the KBr disk technique in the wavelength range from 4000 to 400 cm⁻¹. Moreover, an AXIS-NOVA spectrometer (Kratos Analytical, Ltd., UK) with monochromatic Al K α (1486.71 eV of photons) as the X-ray source was used to study the atomic bonding states of the prevailing elements. Lastly, pH point of zero charge (pH_{pzc}) of the selected best two ACs was measured using the pH drift method described by Sarkar et al. 2019. The results pointed that ZnCl₂-AC and KOH-AC would show neutrality at pH 6.7 and 9.9, respectively (data not shown).

Adsorption evaluations

To examine potential application of the synthesized ACs in dye wastewater treatment, batch adsorption experiments were conducted using MB and MO as model dye pollutants. Firstly, single-point adsorption tests were carried out to check the adsorption capacities of the various AC samples. Next, two best-performed ACs were selected for characterization and further adsorption studies including isotherm and kinetics. The stock solutions (~1200 mg/L) were first prepared and then diluted into working solutions. Approximately 10 mg of the AC samples was weighed into 50-mL falcon tubes, and 20 mL of the dye solutions was added for adsorption. The contents were placed in a multishaking incubator (HB-201MS-2R, Hanbaek, Korea) set to 120 rpm and 25 ± 2 °C for 24 h. The initial concentrations for the isotherm experiments were 0, 50, 100, 200, 400, 700, and 1100 mg/L at pH ranging from 7 to 8 for MB and 3 and 7 for MO adsorption (Mahmoudi et al. 2014). For the kinetic experiments, 300 mL of 100 mg/L dye solutions was filled into glass beakers tightly covered with aluminum foils and placed on multipurpose magnetic stirrers with rod-type stirring bars. AC doses of 0.1 or 0.05 g were then weighed and added to the solutions and a timer was immediately set. Approximately 1 mL of each solution was drawn from the bulk at varying time intervals for 24 h, centrifuged at 12000 rpm, diluted and analyzed using a UV spectrophotometer (UV-2550, Shimadzu, Kyoto, Japan) at 664 and 505 nm for MB and MO, respectively. The equilibrium uptakes, q , were calculated from the mass balance expression in Eq. (1).

$$q = \frac{(C_i - C_e)V}{M} \quad (1)$$

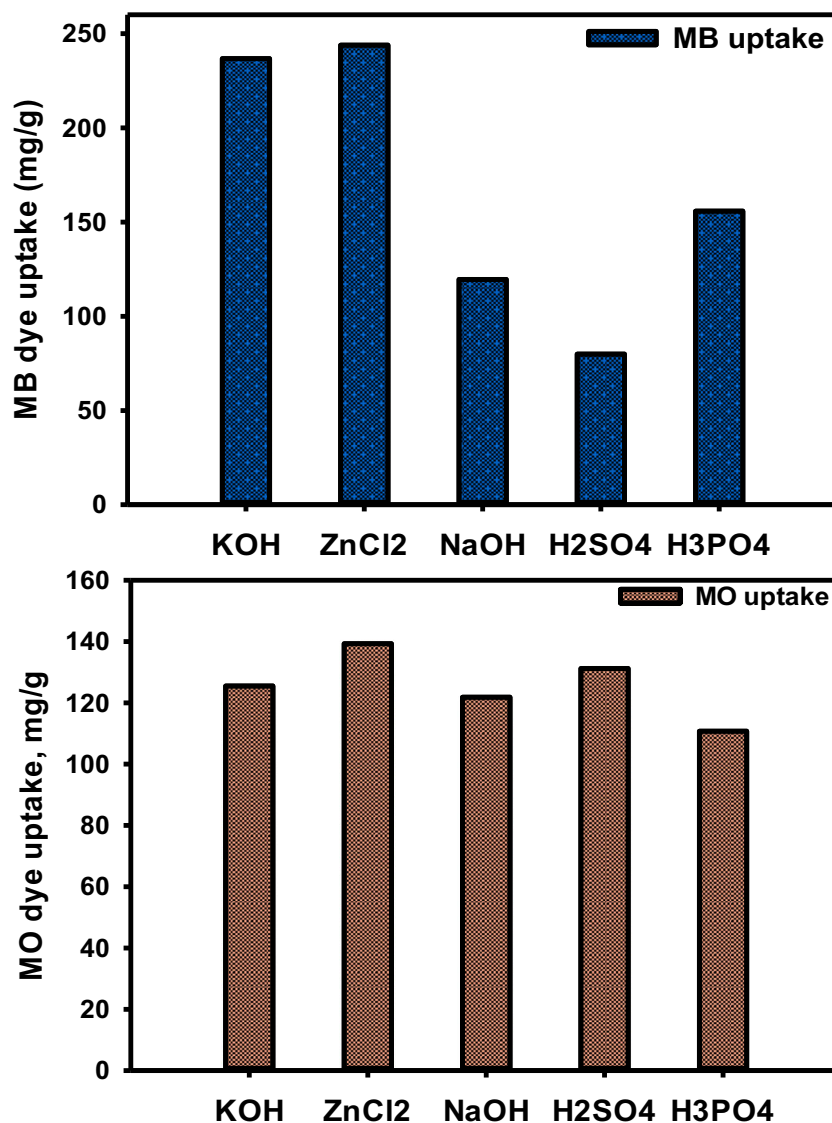
where C_i and C_e are the initial and equilibrium dye concentrations (mg/L), V is the volume of dye (L), and M is the dry mass of AC (g).

Results and discussion

Evaluation of MB and MO dye adsorption capacities

Figure 1 shows the MB and MO dye adsorption results of the ACs prepared with different activation agents, as evaluated through single-point adsorption studies. From the figure, it could be seen that all the ACs exhibited considerable adsorption affinities towards the dyes. However, ZnCl₂-AC showed the best affinities for both dyes, while KOH-AC and H₂SO₄-AC also showed comparable uptakes as ZnCl₂-AC, for MB and MO, respectively. Overall, the orders of uptakes were ZnCl₂-AC > KOH-AC > H₃PO₄-AC > NaOH > H₂SO₄-AC for MB, and ZnCl₂-AC > H₂SO₄-AC > KOH-AC > NaOH > H₃PO₄-AC for MO. The differences in the adsorption trends could be due to the different mechanisms and degrees of

Fig. 1 Single-point adsorption evaluation of the ACs prepared with different activating agents



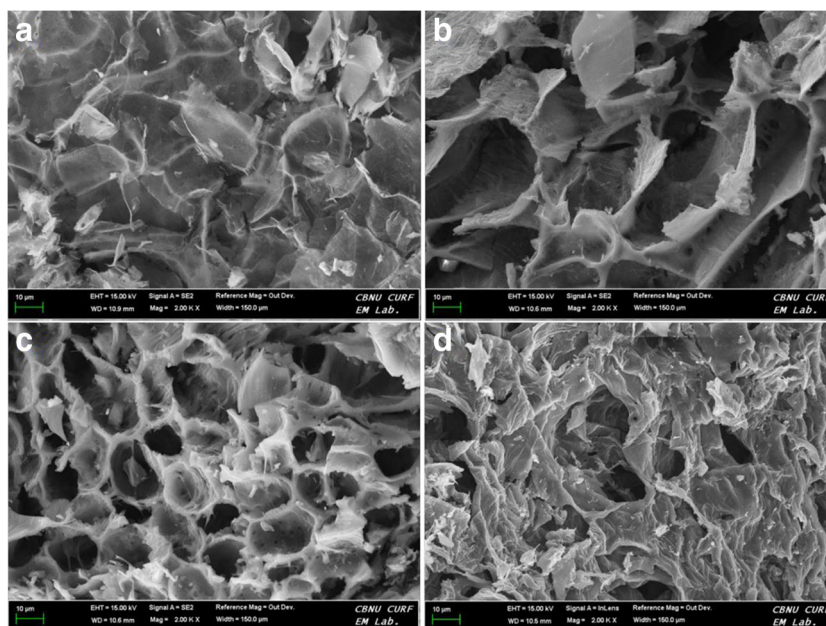
activations by the individual activation agents. According to the literature, carbon activation using metal hydroxides involves etching of the carbon frameworks by redox reactions, formation of H₂O, CO₂ and carbon gasification reactions, and eventual formation of metallic residues that intercalate into the carbon lattices (Abechi et al. 2013; Foo and Hameed 2012; Wang and Kaskel 2012; Zequine et al. 2017). The intercalation causes expansion of the carbon lattices and hence increases the porosity of the ACs. Moreover, the activation processes of acids are said to proceed by initiation of bond cleaving which leads to dehydration, liberation, and elimination of various light and volatile substances, thereby yielding partial aromatization and hence carbonization (Khaled et al. 2009). Thus, the higher uptakes of the prepared ACs could be attributed to the reaction mechanisms described above. Following the preliminary results, the ZnCl₂-AC and KOH-AC were characterized and used for detailed adsorption studies.

Characteristics of the ACs

Morphological and textural characterizations

Figure 2 presents the FE-SEM images of the ZnCl₂-AC and KOH-AC and shows that they possess porous surface morphologies. The micro-pores of the ZnCl₂-AC were, however, more visible on the surface. The surface morphologies experienced slight alterations after the dye adsorption. The surface of the KOH-AC became slightly fluffy, whereas that of the ZnCl₂-AC became wave-like with limited visibility of the earlier visible numerous micro-pores. This could be due to coverages of the adhering dyes on and within the porous surfaces. In both AC materials, interconnected micro-channels were seen as probable migration routes for facilitating rapid adsorption (Sarkar et al. 2019). From the N₂ adsorption curves shown in Fig. 3a, the ZnCl₂-AC exhibited a higher BET surface area and

Fig. 2 FE-SEM images of KOH-AC **a** before and **b** after MB adsorption and ZnCl₂-AC **c** before and **d** after MB adsorption



N₂ adsorption capacity (1439.50 m²/g, 0.331 cm³ STP/g) than the KOH-AC (1370.76 m²/g, 0.283 cm³ STP/g), an obvious validation of its higher degree of micro-porosity as evident from Fig. 2 and the inset of Fig. 3a.

Crystallinity and functional group analyses

The crystallinity of an AC is helpful for determining its structural or backbone orientation and degree of graphitization. The KOH-AC and ZnCl₂-AC samples showed broad humps at 2θ = 24° and 43°, which are characteristics of the cellulosic backbone of the pristine biomass and graphitic structures of the carbon frameworks, respectively (Fig. 3b) (Bediako et al. 2017, Bediako et al. 2015, Chen et al. 2010a, b, Huang et al. 2011, Nekouei et al. 2016, Sun et al. 2008). Besides, a sharp and high-intensity graphite-like peak appeared at 28.9° in the spectrum of the KOH-AC, an indication that a higher degree of graphitization had occurred in its structure (Chen et al. 2010a, b; Huang et al. 2011; Nekouei et al. 2016; Sun et al. 2008). The peak, however, experienced drastic reduction in intensity after the MB dye adsorption. In addition, several low-intensity amorphous-like peaks were observed which may be due to edge defects in the carbon structures (Lagerge et al. 1999).

Furthermore, distinct peaks mainly belonging to the hydroxyl, amine, carboxyl, and carbonyl functional groups were observed in the FTIR spectra of the samples (Fig. 3c). That is, the strong stretching vibrational peaks emerging around 3451 cm⁻¹ were attributed to overlapping of the O–H and N–H bands (Li et al. 2013; Tang et al. 2017). The bands at ca. 1637 cm⁻¹ were due to asymmetric stretching vibrations of the C=O groups (Bediako et al. 2015; Bediako et al. 2016c;

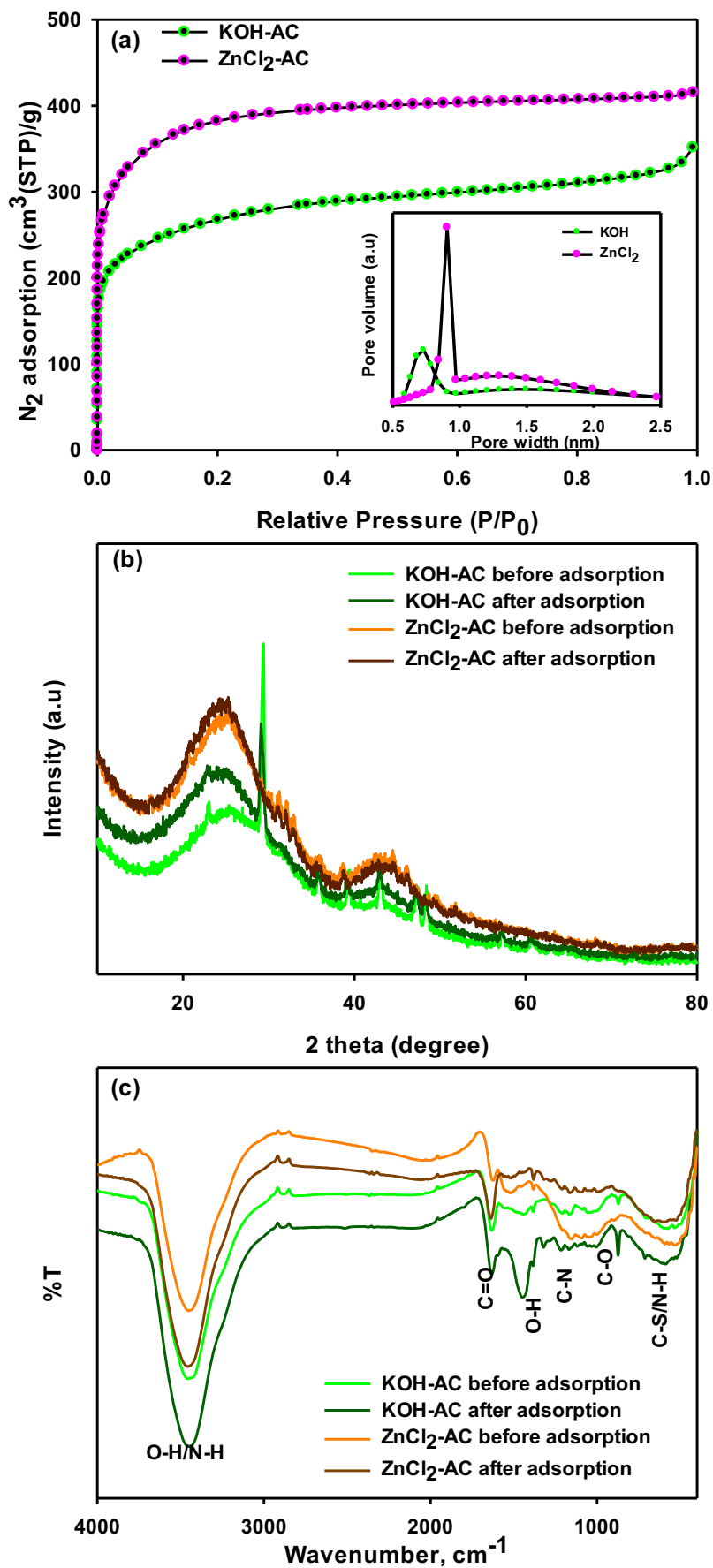
Tang et al. 2017). In addition, the bands at 1446, 1218, and 1004 cm⁻¹ were assigned to the presence of O–H, C–N, and C–O stretching vibrations, respectively (Bankar et al. 2010; Bediako et al. 2016c; Liu et al. 2016). Finally, the stretch of bands between 890 and 517 cm⁻¹ reflects C–S bending vibrations and N–H deformation of amines (Bediako et al. 2015; Memon et al. 2008). The presence of vast varieties of functional groups was not unexpected owing to the nitrogen environment employed in the synthesis, coupled with the complex composition of the orange peel biomass precursor.

Adsorption studies

Adsorption kinetics

Adsorption kinetics is helpful for determining the phenomenological coefficients that characterize the transport of adsorbates within adsorbents (Azizian 2004; Bediako et al. 2016a). It is crucial to define the rate of adsorption from the bulk medium onto the surfaces of the adsorbents. Figure 4 a shows the adsorption kinetics of MB and MO adsorption. The adsorption rates were swifter at the beginning of the adsorption process owing to the ready availability of binding sites but became quite sluggish towards equilibrium, due to exhaustion and lack of easy access to the binding sites (Anirudhan et al. 2012; Bediako et al. 2016b). The KOH-AC required about 6 h to reach adsorption equilibrium for MB, while the ZnCl₂-AC required a little over 20 h to achieve same for MB but took a relatively shorter time of only 4 h for MO. The continuous rising nature of the data points for MB adsorption by the ZnCl₂-AC likely delayed its equilibrium time. Thus, since the dyes have similar dimensions (Xu et al. 2018), the

Fig. 3 **a** N₂ adsorption isotherms, **b** XRD patterns, and **c** FTIR spectra of the AC samples



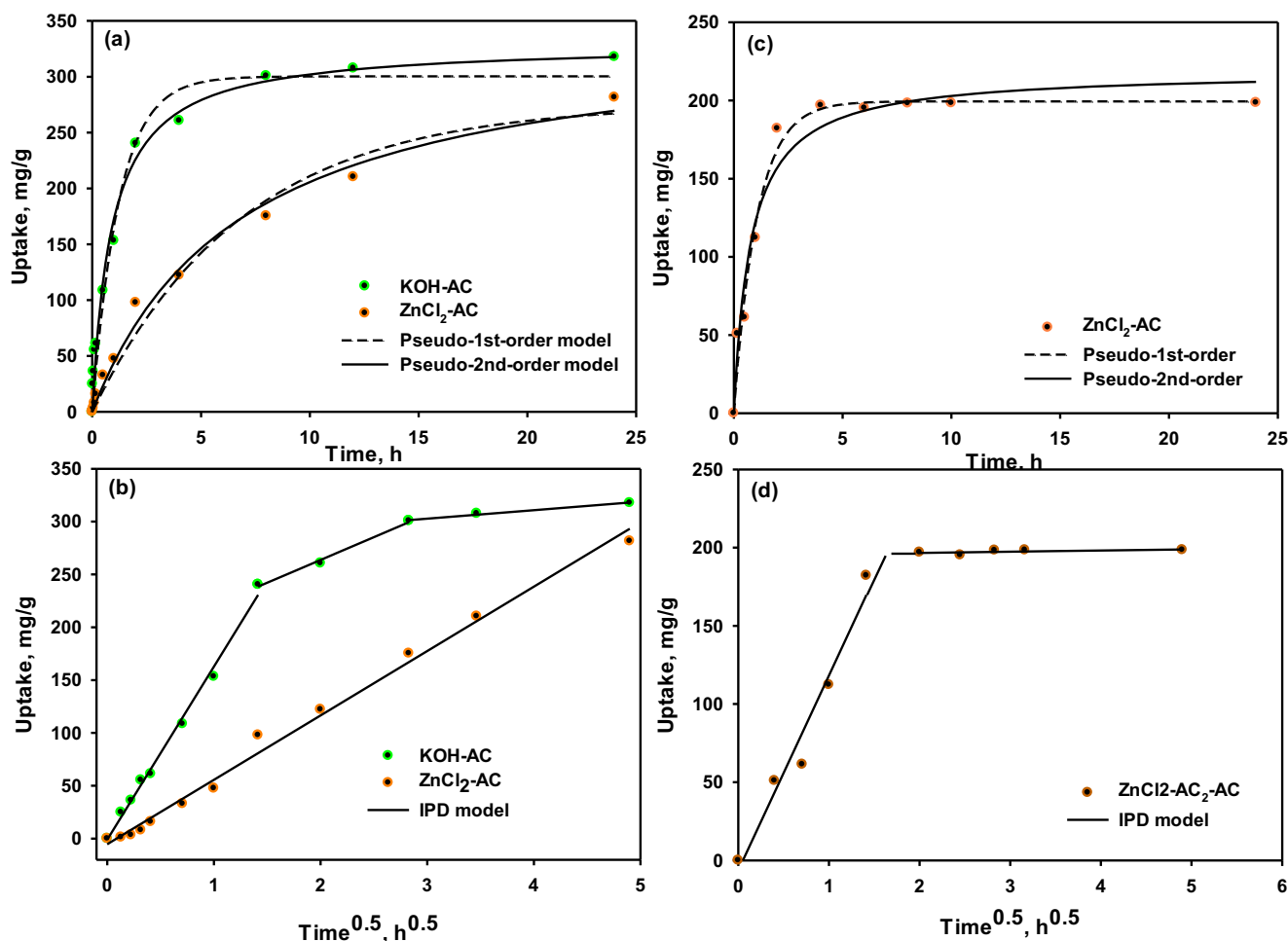


Fig. 4 Results of **a** kinetics and **b** intra-particle diffusion modeling for MB adsorption using KOH-AC and ZnCl₂-AC and **c** kinetics and **d** intra-particle diffusion modeling for MO adsorption using ZnCl₂-AC

differences in reaching the adsorption equilibrium could be due to adsorption affinity differences by the ACs and the mechanisms involved, rather than size difference of the dyes.

The pseudo-first-order (Bhattacharya and Venkobachar 1984) and pseudo-second-order (Ho and McKay 1999) models were used to fit the kinetics data, and the model equations are given by Eq. (2) and Eq. (3), respectively.

$$q_t = q_1(1 - \exp(-k_1 t)) \tag{2}$$

$$q_t = \frac{q_2^2 k_2 t}{1 + q_2 k_2 t} \tag{3}$$

where q_t is the uptake (mg/g) at time, t ; q_1 and q_2 are the uptakes at equilibrium (mg/g); and k_1 and k_2 are the pseudo-first-order and pseudo-second-order rate constants, respectively.

The pseudo-first-order model defines the adsorption interaction between the solid ACs and dye solution based on the adsorption capacity of the ACs by assuming that one dye molecule will occupy only one adsorption site (Bediako et al. 2016a; Boparai et al. 2011). The pseudo-second-order

model, on the other hand, examines the chemisorption kinetics of the ACs from the liquid dye solution (Azizian 2004; Ho 2006). From the model parameters summarized in Table 1, it could be observed that both but the pseudo-second-order model provided a better representation of the data in most instances, which is consistent with the results obtained by some other authors for dye adsorption (Li et al. 2013; Ofomaja 2007; Sarkar et al. 2015; Mahmoudi et al. 2014). The proximity in the estimated coefficient of correlation, R^2 values for both kinetic models thus suggest that a combination of chemical and electrostatic interactions were likely involved in the adsorption process and that there were strong interactions between the dyes and functional groups present on and within the AC samples (Bediako et al. 2016c; Boparai et al. 2011; Qi et al. 2013).

To understand the diffusion mechanisms involved in the adsorption process, the kinetic data were further examined with the intra-particle diffusion (IPD) model which is represented by Eq. (4).

$$q_t = k_i t^{0.5} + C_i \tag{4}$$

Table 1 Kinetic parameters for MB and MO adsorption by KOH-AC and ZnCl₂-AC

Adsorbent	$q_{exp,t}$	Pseudo-1st-order			Pseudo-2nd-order		
		q_1 (mg/g)	k_1 (1/min)	R^2	q_2 (mg/g)	k_2 (g/mg min)	R^2
KOH-AC for MB	317.70	300.32 ± 10.55	0.81 ± 0.011	0.976	329.63 ± 10.02	0.004 ± 0.0005	0.988
ZnCl ₂ -AC for MB	281.52	275.75 ± 16.27	0.15 ± 0.02	0.981	326.07 ± 19.90	0.004 ± 0.0002	0.991
ZnCl ₂ -AC for MO	198.51	199.47 ± 5.16	0.932 ± 0.11	0.981	218.84 ± 9.91	0.006 ± 0.001	0.964

where k_i is the intra-particle diffusion rate constant, and C_i is the intercept representing the thickness of the boundary layer (Kim et al. 2015; Li et al. 2013). The IPD model parameters given in Table 2 were obtained from the plot of q_t versus $t^{0.5}$. According to this model, the adsorption process is assumed to be associated with IPD if the regression of the above plot is linear, and if the regression line passes through the origin, then IPD becomes the sole rate-controlling step of the reaction (Kim et al. 2015; Li et al. 2013; Won et al. 2013). The plot of q_t versus $t^{0.5}$ showed multilinear characteristics for the MB adsorption by KOH-AC, revealing that three steps were involved in the adsorption process (Fig. 4b). The first sharp portion is the external surface adsorption or instantaneous adsorption stage where the adsorption was swifter with higher uptake (larger slope), the second subdued section is the gradual adsorption or transition stage, and the third section is the final equilibrium phase where intra-particle diffusion controlled the rate of adsorption (Bediako et al. 2019a; Li et al. 2013; Won et al. 2013).

Conversely, the MB adsorption by ZnCl₂-AC exhibited a single linear phase passing through the origin and suggested IPD as the sole rate-limiting step. Since the IPD mechanism involves time-dependent transport of dye from the bulk surface into the inner cavities of the AC adsorbents, the slower MB adsorption rate of the ZnCl₂-AC could be understood. For the MO adsorption, however, the ZnCl₂-AC showed two phases of instantaneous external adsorption, followed by the final equilibrium phase. This swift switch from instantaneous to equilibrium adsorption explains the reason why the MO adsorption was the fastest to reach equilibrium. Moreover, the dimensions of the MB are approximated as 0.17 wide × 0.76 high × 0.33 nm thick (Arias et al. 1999), and those of MO are 0.18 wide × 0.76 high × 0.60 nm thick (Xu et al. 2018). These size

dimensions make it possible for easy penetration of the dyes into the AC pores which are about the mean size 0.7–1.5 nm.

Adsorption isotherms

Adsorption isotherm is important in adsorption studies because it helps to describe the interactive behaviors of adsorbents and adsorbates, as well as estimating the maximum adsorption capacities (Li et al. 2014; Park et al. 2018). By definition, it represents the amount of species bound onto the surface of adsorbents as a function of the remaining species in solution (Bediako et al. 2016c). The results of the adsorption isotherm experiments as fitted to several adsorption models as shown in Fig. 5. Both the KOH-AC and ZnCl₂-AC showed similar adsorption trends for MB and MO. In other words, the isotherm data points followed the usual adsorption phenomenon where the adsorption capacity increases with increasing initial concentration and reaches a near plateau-like shape at equilibrium (Liang et al. 2009; Pillai et al. 2013).

To statistically analyze the results, the experimental data were exported from excel to Sigma Plot software (version 12.0, SPSS, USA) and fitted via the Langmuir (Langmuir 1918), Freundlich (Freundlich 1906), Redlich–Peterson (R–P) (Bediako et al. 2017), Temkin (Dada et al. 2012), and Sips (Nethaji et al. 2013) isotherm models which are expressed by Eq. (5) through Eq. (9).

$$\text{Langmuir model : } q_e = q_m \frac{bC_e}{1 + bC_e} \quad (5)$$

where q_m is maximum uptake at equilibrium (mg g⁻¹), b is the coefficient corresponding to the affinity between the

Table 2 Intra-particle diffusion model parameters

Adsorbent	Phase	Intraparticle diffusion		
		k_i (mg g ⁻¹ min ^{0.5})	C	R^2
KOH-Activated carbon for MB	1st	163.73 ± 5.46	− 0.01 ± 0.37	0.994
	2nd	43.15 ± 3.80	177.41 ± 8.21	0.992
	3rd	8.00 ± 0.83	278.80 ± 3.21	0.989
ZnCl ₂ -activated carbon for MB	1st	60.97 ± 1.66	− 0.02 ± 0.43	0.998
ZnCl ₂ -activated carbon for MO	1st	124.70 ± 14.07	− 6.52 ± 0.37	0.963
	2nd	0.77 ± 0.51	195.10 ± 1.84	0.984

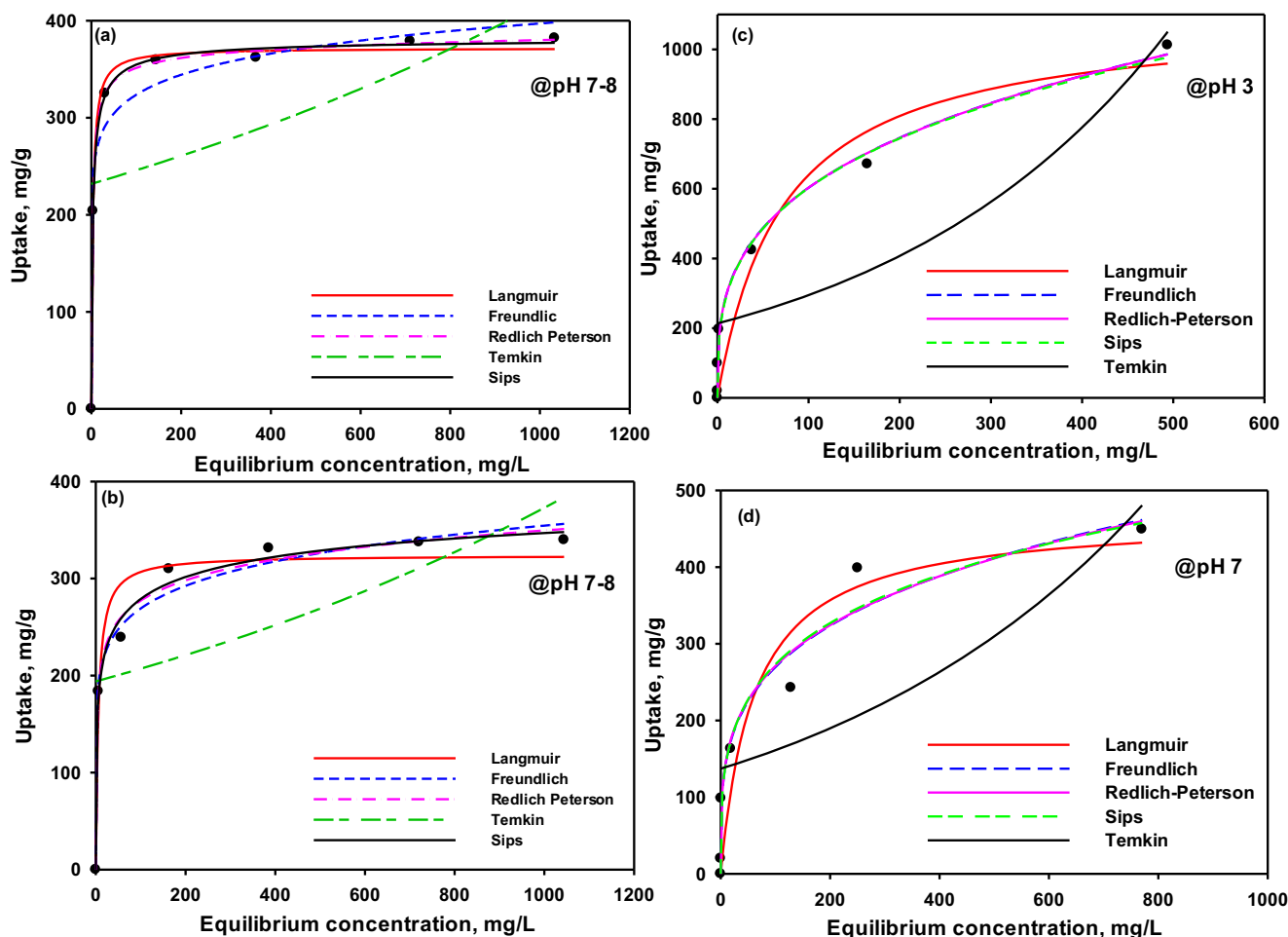


Fig. 5 Isotherm of MB dye adsorption by a KOH-AC and b ZnCl₂-AC and MO adsorption at c pH 3 and d pH 7 by ZnCl₂-AC

adsorbent and adsorbate, q_e is the equilibrium uptake (mg g^{-1}), and C_e is the equilibrium concentration of adsorbate (mg L^{-1}).

$$\text{Freundlich model : } q_e = KC_e^{1/n} \tag{6}$$

where K and n are the Freundlich constants denoting the relative adsorption capacity and adsorption intensity, respectively. The Langmuir model depicts a monolayer adsorption phenomenon of adsorbates onto adsorbents at specific homogeneous sites, while the Freundlich model describes both monolayer and multilayer adsorption onto heterogeneous surfaces (Bediako et al. 2016a; Pillai et al. 2013).

$$\text{Redlich–Peterson model : } q_m = K_{RP} \frac{C_f}{1 + a_{RP} C_f^{\beta_{RP}}} \tag{7}$$

where K_{RP} and a_{RP} are the Redlich–Peterson isotherm constants (L/mg) and β_{RP} is the Redlich–Peterson model exponent which values range between 0 and 1. The model tends to follow the Langmuir model when the R–P constant is 1 or close to 1 and assumes the

Freundlich model when R–P constant is (zero) 0 or close to zero (Bediako et al. 2017).

$$\text{Temkin model : } q_e = \frac{RT}{b} \ln(A_T b C_e) \tag{8}$$

where A_T is the Temkin isotherm equilibrium binding constant (L/g), b_T is the Temkin isotherm constant, R is the universal gas constant (8.314 J/mol/K), and T is temperature at 298 K.

$$\text{Sips model : } q_m = \frac{q_m (K_{RP} C_e)^{n_s}}{1 + (K_{RP} C_e)^{n_{RP}}} \tag{9}$$

where K_S (L/mg) represents the affinity constant and n_S indicates the surface heterogeneity. When n_S approaches unity, the Sips isotherm assumes the Langmuir isotherm and predicts adsorption at homogeneous sites. Conversely, deviation of the n_S value away from unity suggests heterogeneous surface adsorption.

As can be seen from the model parameters displayed in Table 3, all models except the Temkin model fitted the isotherm data with very high R^2 values exceeding 0.90. Particularly, the Sips and Langmuir models predicted the

maximum equilibrium uptakes quite well, thus depicting mixed monolayer and multilayer adsorptions onto the surfaces of the ACs. This is however not unexpected because it is a common characteristics of activated carbons (Tran et al. 2017). Furthermore, the ACs exhibited stronger affinity and adsorption intensity for MB than MO as can be observed from the initial slopes of the isotherm curves in Fig. 5 and the model parameters in Table 3. The better MB affinity of the ACs did not necessarily translate into higher equilibrium uptakes because adsorption is a time-dependent process. Moreover, a higher equilibrium MO uptake was obtained at pH 3 than obtained at pH 7. This was due to the pH_{pzc} of the $ZnCl_2$ -AC which is 6.7. It presupposes that the surface of the AC would be positively charged at pH 3 and, hence, could effectively interact with the negatively charged MO, leading to a higher adsorption through electrostatic binding.

Comparison of adsorption performances and practical adsorption evaluation

A compilation of recently reported adsorbents, mostly from agro-waste-derived carbons is summary in Table 4. Like in the present study, most of the previous reports performed detailed characterization and textural analysis of the prepared adsorbents, conducted the adsorption experiments at defined environmental conditions (such as pH, temperature, time, and stirring/shaking speed), and examined the experimental data with several isotherm and kinetic models. However, only a handful of researchers performed thermodynamic and regeneration studies. *Ceteris paribus*, the adsorption performances of the synthesized ACs, especially for MO, far outweighed

most of the reported works, which suggests that the prepared ACs are superior competitors for application.

To test applicability of the ACs in treating dyes on industrial scale, an organic wastewater sample containing MB was collected from the Environmental Biotechnology National Research Laboratory in Chonbuk National University. After initial analysis using UV, the concentration of MB was determined to be ~ 35 mg/g. Subsequently, the $ZnCl_2$ -AC and KOH-AC were separately contacted with measured volumes of the organic wastewater sample. After few hours, the blue-colored solutions became colorless to the unaided eye (Fig. 6), indicating complete removal of the MB dye. After UV analysis, the removal efficiencies were found to be greater than 99% for each of the two ACs.

XPS analysis and mechanisms of adsorption

XPS is an important characterization tool for identifying the presence and composition of elements and bond types in materials (Dambies et al. 2001; Zhou et al. 2005). The results from XPS could provide key information on the adsorption mechanisms of the dye molecules. Thus, using the KOH-AC and MB as representative carbon and dye, respectively, the high resolution core-level spectra of the prevailing C, N, and S atoms were deconvoluted into separate peaks as displayed in Fig. 7. Before the deconvolution, each spectrum was calibrated to the C1s peak at 284.6 eV (Wagner 1979). The S2p spectra showed no prevailing S peaks prior to the MB adsorption, indicating that no sulfur groups were initially present on the surface of the AC. After adsorption, however, a pair of peaks corresponding to the $S2p_{3/2}$ and $S2p_{1/2}$ orbitals of S with

Table 3 Modeled isotherm parameters for dye adsorptions by KOH- and $ZnCl_2$ -activated carbons

Isotherm model	Parameter	Adsorbent			
		KOH-AC (MB)	$ZnCl_2$ -AC (MB)	$ZnCl_2$ -AC (MO@pH 3)	$ZnCl_2$ -AC (MO@pH 7)
Langmuir	q_{max}^{exp} (mg/g)	382.15 ± 8.62	339.82 ± 6.98	1012.10 ± 29.13	449.18 ± 17.45
	q_{max}^{calc} (mg/g)	378.89 ± 4.61	334.07 ± 14.32	1098.60 ± 62.14	466.06 ± 22.32
	b (L/mg)	0.328 ± 0.035	0.177 ± 0.065	0.014 ± 0.003	0.016 ± 0.002
	R^2	0.996	0.979	0.938	0.903
Freundlich	k (L/g) ^{1/n}	215.22 ± 22.96	115.11 ± 14.36	146.12 ± 818.09	80.21 ± 18.50
	n	11.27 ± 2.37	8.36 ± 1.10	3.25 ± 0.23	3.80 ± 0.57
	R^2	0.971	0.976	0.994	0.968
Redlich-Peterson	K_{RP} (L/mg)	150.82 ± 10.97	193.1534 ± 18.22	317.76 ± 14.32	419.24 ± 31.04
	α_{RP} (L/mg)	0.47 ± 0.046	1.07 ± 0.198	2.18 ± 0.76	0.59 ± 0.03
	β_{RP}	0.98 ± 0.005	0.91 ± 0.009	0.69 ± 0.03	0.74 ± 0.05
	R^2	0.999	0.989	0.994	0.952
Temkin	a_T (L/g)	0.0006 ± 0.0004	0.0007 ± 0.0004	0.0032 ± 0.0009	0.0016 ± 0.0006
	b_T (J/mol)	10.68 ± 2.78	12.77 ± 3.33	11.39 ± 4.49	17.77 ± 6.58
	R^2	0.311	0.383	0.738	0.584
Sips	q_m (mg/g)	382.77 ± 5.35	442.35 ± 11.52	1077.11 ± 52.62	422.48 ± 9.75
	K_s (L/mg)	0.34 ± 0.031	0.05 ± 0.013	0.17 ± 0.03	0.96 ± 0.06
	A_s (L/mg)	0.72 ± 0.073	0.33 ± 0.046	0.32 ± 0.06	0.29 ± 0.02
	R^2	0.999	0.992	0.992	0.967

Table 4 Comparison of dye adsorption performances of various biomass-based carbon adsorbents

Adsorbent	Chemical treatment	Dye	EP	SSA (m ² /g), TPV (cm ³ /g)	Uptake (mg/g)	Isotherm/kinetic models	AE (kJ/mol)	Reference
Orange peel carbon	KOH activated	MB	pH 7–8, 25 ± 2 °C, 120 rpm, 24 h	1370.76, 0.283	317.70	LM, FM, RPM, TM, SM/PFO, PSO, IPD	–	This work
Orange peel carbon	ZnCl ₂ activation	MB	pH 7–8, 25 ± 2 °C, 120 rpm, 24 h	1439.50, 0.331	281.52	LM, FM, RPM, TM, SM/PFO, PSO, IPD	–	This work
Orange peel carbon	ZnCl ₂ activation	MO	pH 3 and 7, 25 ± 2 °C, 120 rpm, 24 h	1439.50, 0.331	1097.3 (pH 3), 402.2 (pH 7)	LM, FM, RPM, TM, SM/PFO, PSO, IPD	–	This work
Activated mesoporous chitosan carbon aerogel	Nitrogen doping	MO	–, 25 °C, –, 180 min	554.1, 0.747	400	LM, FM, TM/PFO, PSO, IPD	31.32	Jiang et al. (2019)
Açaí biochar	NaOH activation	MB	pH 5.5, 25 °C, 300 rpm, –	491.90, 0.315	93.23	FM, LFM, TM, MLM, DLM/PFO, PSO, PNO	–14.94	Pessôa et al. (2019)
<i>Anomalocardia brasiliensis</i> shellfish shells	Thermal activation at 1000 °C	Nylosan Brilliant Blue acid	pH 12.4, 25 °C, 450 rpm, 120 min	4.44, 1.03 × 10 ⁻³	405	LM, FM, LFM/PFO, PSO, IPD	–23.79	de Paiva et al. (2018)
Commercial activated carbon	copper sulfide nanoparticles loading	MO	pH 5, 25 °C, 400 rpm, 4 min	1286, 545 × 10 ⁻⁶	122	Several models	–	Mokhtari et al. (2016)
Buriti shell carbon	ZnCl ₂ activation	MB	–, –, 220 rpm, 180 min	843, 0.490	274.62	LM, FM, RPM/PFO, PSO, IPD, EM	–	Pezoti et al. (2014)
xGnP® graphite nanoplatelets	No activation	DDB	pH 3.5, 25 °C, 150 rpm, 120 min	118.19, –	22.14	LM, FM/PFO, PSO	–27.01	Oliveira et al. (2019)
Alginate molded Clay beads	H ₂ SO ₄ treatment and calcination	DR80	–, 30 °C, 140 rpm, 24 h	92, 0.2183	38.36	LM, FM, RPM/PFO, PSO	–20.71	Auta and Hameed (2012)
Sucrose	Hydrothermal treatment and KOH activation	CH	–, 25 °C, 150 rpm, 2.5–240 min	1534, 0.765	28.68	LM, FM, RPM, DRM/PFO, PSO, IPD, EM	–111.10	Bedin et al. (2016)
Orange peel carbon	Carbonization and K ₂ CO ₃ activation	MB	–, 30 °C, 120 rpm, –	1104.45, 0.615	156.77	LM, FM, RPM, ToM, DRM/PFO, PSO, EM	–12.09	Foo and Hameed (2012)
<i>Phragmites australis</i> activated carbon	H ₃ PO ₄ activation	MO	Natural pH, 22 ± 2 °C, 150 rpm, 240 min	1362, 1.27	238.10	LM, FM, TM/PFO, PSO, EM	–	Chen et al. (2010a, b)
Cotton stalk	No treatment	MV	~ pH 7, 35 °C, 160 rpm, 3 h	–	476.19	LM, FM, TM/PFO, PSO, IPD	–	Deng et al. (2011)
Wood biochar	Gasification	Indosol Black NF1200	pH 2 and 12, 28 °C, 200 rpm, 200 min	350.4, –	147.06	LM, FM, TM/PFO, PSO, IPD	–	Kelm et al. (2019)
Cotton stalk	H ₂ SO ₄ treatment	MB	~ pH 7, 35 °C, 160 rpm, 3 h	2.81, 0.006	12 (pH 2), 185 (pH 12)	LM, FM, TM/PFO, PSO, IPD	–	Deng et al. (2011)
Cotton stalk	H ₃ PO ₄ treatment	MB	~ pH 7, 35 °C, 160 rpm, 3 h	7.27, 0.015	222.22	LM, FM, TM/PFO, PSO, IPD	–	Deng et al. (2011)
Multiwalled carbon nanotubes	Chemical vapor deposition	MO	pH 7, 25 °C, 2 h	160, 0.67	51.74	LM, FM, TM/PFO, PSO, IPD	19.39	Yao et al. (2011)
exf.LT/AP-g-p(DEAEMA)	In situ polymerization	MB	pH 9, 30 °C, –, 12 min	125.94, –	599	LM, FM/PSO, IPD	23.15	Sarkar et al. (2015)
Coconut coir activated carbon	Carbonization and ZnCl ₂ activation	MB	–, 30 °C, 150 rpm, 100 min	205.27, 0.025	15.59	LM, FM/PFO, PSO	–	Sharma et al. (2010)
Date pits activated carbon	ZnCl ₂ activation	MO	pH 3.5, 25 °C, 100 rpm, 4 h	1380, 0.91	434	LM, FM/PFO, PSO	–	Mahmoudi et al. (2014)
Date pits activated carbon	ZnCl ₂ activation	MB	pH 9, 25 °C, 100 rpm, 4 h	1380, 0.91	455	LM, FM/PFO, PSO	–	Mahmoudi et al. (2014)

Table 4 (continued)

Adsorbent	Chemical treatment	Dye	EP	SSA (m ² /g), TPV (cm ³ /g)	Uptake (mg/g)	Isotherm/kinetic models	AE (kJ/mol)	Reference
GO/Ca-alginate	Immobilization	MB	pH 5.4, 25 °C, 5 h	–	181.81	LM, FM/PFO, PSO, IPD	–5.27	Li et al. (2013)
Regenerated activated carbon	Microwave treatment	MB	pH 7, 20 °C, –, 0.5–5 h	1560, 0.96	425.53	LM, FM/PFO, PSO, IPD	–	Zhang et al. (2010)

EP environmental parameters, *SSA* specific surface area, *AE* adsorption enthalpy, *LM* Langmuir model, *FM* Freundlich model, *RPM* Redlich–Peterson model, *TM* Temkin model, *ToM* Toth model, *SM* Sips model, *LFM* Langmuir–Freundlich model, *MLM* monolayer single energy model, *DLM* double layer-two energy site model, *PFO* pseudo-first-order model, *PSO* pseudo-second-order model, *IPD* intra-particle diffusion model, *EM* Elovich model, *DRM* Dubinin–Radushkevich model, *PNO* pseudo-*n*-order model

a distance of 1.2 eV apart was observed (Liu et al. 2013; Squarzialupi et al. 2002). These observed S peaks were assigned to the sulfur atom in the MB structure and indicated that the adsorbed dye was stabilized on the AC. Furthermore, a huge bump of doped N atom was seen in the spectrum of the AC before adsorption; however, the intensity had increased significantly after adsorption. Similar to the S peaks, the increase in intensity likely resulted from the N atom contained in the structure of the MB dye (Patel et al. 2015). Thus, the presence of the S and N peaks following the MB dye adsorption signified effective binding and retention of the dye on the surface of ACs.

In the case of the deconvoluted C1s spectra, several bond peaks were observed. These peaks include C–C/C=C, C–N, C–O, C=O/O–C=O, and pi–pi* excitation (Dementjev et al. 2000; Wang et al. 2018). Noteworthy, the intensity of the C–N peak had significantly increased, and a new peak corresponding to C–S/C=S had emerged after adsorption (Wagner 1979). Moreover, the pi–pi* excitation peak had not only shifted to a lower binding energy state from 293.15 to 292.10 eV but had also experienced a significant reduction in intensity. The above observations pointed to the adsorption process likely involving mechanisms such as pi–pi interactions, electrostatic attractions, non-electrostatic hydrogen bond formations, and electron donor–acceptor reactions (Song et al. 2019; Vargas et al. 2011). The pi–pi interactions were possible between the aromatic ring of the MB and the aromatic structure of the graphite-like layers of the ACs. As already discussed under the XRD characterization, the ACs exhibited graphitic carbon peaks and thus graphitic behavior. Moreover, electrostatic attractions between the N atom of the MB dye and the anionic functional groups such as the carboxyl groups on the ACs was possible because the N atoms are reported to assume positive charges at pH ~ 8 where the adsorption experiments were conducted (Bediako et al. 2019b; Sarkar et al. 2019). In addition, the hydroxyl group of AC and terminal nitrogen of MB dye could undergo a non-electrostatic

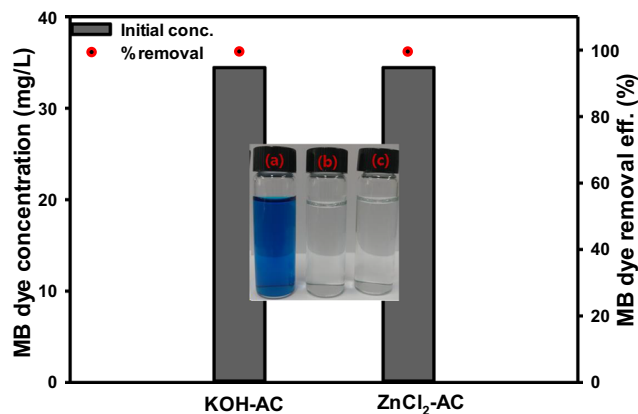


Fig. 6 MB adsorption evaluation of ZnCl₂-AC and KOH-AC from laboratory organic wastewater

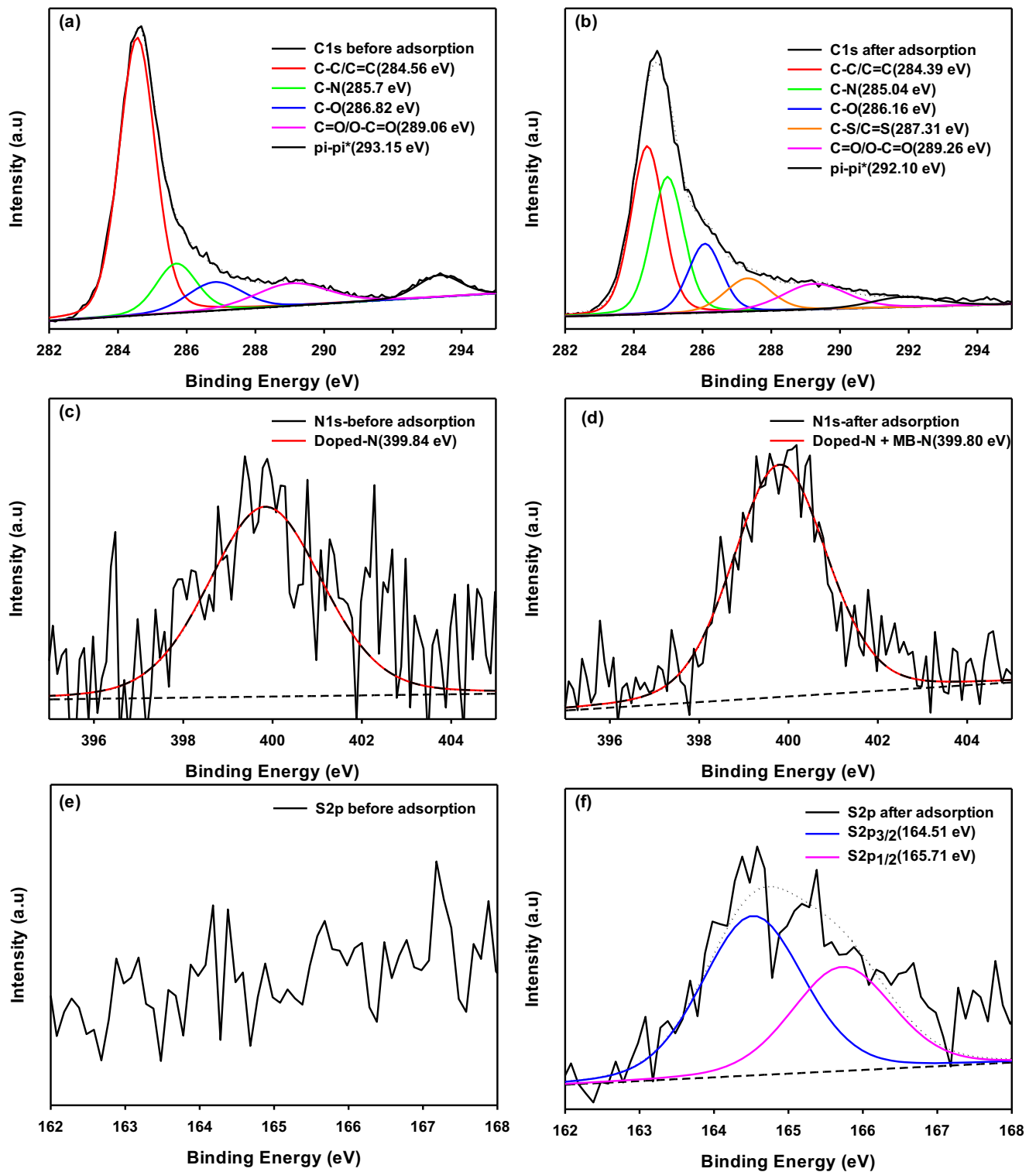


Fig. 7 XPS deconvoluted spectra of KOH-AC: C1s a before and b after, N1s c before and d after and S2p e before and f after MB adsorption

hydrogen bond formation reaction, while the carbonyl oxygen of the AC and aromatic ring of the MB dye would engage in an electron donor–acceptor process (Moreno-Castilla 2004; Vargas et al. 2011). The above-discussed interactions are also expected for the MO adsorption, except that the electrostatic

interaction would be between the deprotonated sulfonate groups and positively charged nitrogen groups on the ACs (Mahmoudi et al. 2014; Fraga et al. 2018). By these mechanisms, the effective adsorption and retention of the adsorbed dyes on the ACs could be well comprehended.

Conclusions

Orange peel ACs were synthesized via activation with H_2SO_4 , NaOH , KOH , ZnCl_2 , and H_3PO_4 . ZnCl_2 -AC showed the highest MB and MO adsorption capacities, with a faster kinetics of MO adsorption of 4 h. KOH -AC, on the other hand, displayed a faster MB adsorption equilibrium (6 h) than the ZnCl_2 -AC (~20 h). The adsorption capacities obtained with the prepared ACs were higher than most recently reported values. Based on the characterization results, the adsorption mechanisms were proposed to include electrostatic attractions, π - π interactions, hydrogen bond formations, electron donor-acceptor reactions, and intra-particle diffusion. Finally, the ACs functioned effectively when applied to MB scavenging from a laboratory organic wastewater, where more than 99% removal efficiency was obtained. Therefore, this work not only does suggest agro-waste orange peel as an AC precursor in lieu of commercial ACs but also provides backgrounds for understanding the adsorptive interactions leading to effective removal of dyes from polluted waters.

Acknowledgments The authors wish to acknowledge the Chonbuk National University's Center for University-wide Research Facility (CURF), especially Mr. Kim Seok Jun and Ms. Song Min-kyeong for assisting with the XRD and FE-SEM analyses, respectively. Final appreciations go to Ms. Chin Narae (Soletek Trading Co., Ltd., Seoul, Korea) and Dr. Kim Hyun Sook of Wongwang University (Iksan, Korea) for assisting with the BET and XPS measurements, respectively.

Funding information This study was supported by the Korean Government through the National Research Foundation, NRF (2017R1A2A1A05001207) grant.

References

- Abechi SE, Gimba CE, Uzairu A, Dallatu YA (2013) Preparation and characterization of activated carbon from palm kernel shell by chemical activation. *Res J Chem Sci* 3:54–61
- Adegoke KA, Bello OS (2015) Dye sequestration using agricultural wastes as adsorbents. *Water Resour Ind* 12:8–24
- Albarelli JQ, Rabelo RB, Santos DT, Beppu MM, Meireles MAA (2011) Effects of supercritical carbon dioxide on waste banana peels for heavy metal removal. *J Supercrit Fluid* 58:343–351
- Anirudhan TS, Fernandez NB, Mullassery MD (2012) Removal of Cd(II) ions from aqueous solution using a cation exchanger derived from banana stem. *J Chem Technol Biotechnol* 87:714–722
- Arias M, López E, Nuñez A, Rubinos D, Soto B, Barral MT, Díaz-Fierros F (1999) Adsorption of methylene blue by red mud, an oxide-rich byproduct of bauxite refining. In: Berthelin J., Huang P.M., Bollag JM., Andreux F. (eds) *Effect of mineral-organic-microorganism interactions on soil and freshwater environments*. Springer, Boston, 361–365
- Armando N, Spreen TH, Jauregui C (2001) The citrus industry of Cuba: 1994–1999. Forthcoming international working paper, Food and Resource Economics Department, University of Florida, Gainesville
- Autá M, Hameed BH (2012) Modified mesoporous clay adsorbent for adsorption isotherm and kinetics of methylene blue. *Chem Eng J* 198–199:219–227
- Azizian S (2004) Kinetic models of sorption: a theoretical analysis. *J Colloid Interf Sci* 276:47–52
- Bankar A, Joshi B, Kumar AR, Zinjarde S (2010) Banana peel extract mediated novel route for the synthesis of silver nanoparticles. *Colloids Surf A Physicochem Eng Asp* 368:58–63
- Bediako JK, Wei W, Kim S, Yun Y-S (2015) Removal of heavy metals from aqueous phases using chemically modified waste Lyocell fiber. *J Hazard Mater* 299:550–561
- Bediako JK, Kim S, Wei W, Yun YS (2016a) Adsorptive separation of Pb(II) and Cu(II) from aqueous solutions using as-prepared carboxymethylated waste Lyocell fiber. *Int J Env Sci Tec* 13:875–886
- Bediako JK, Wei W, Yun Y-S (2016b) Conversion of waste textile cellulose fibers into heavy metal adsorbents. *J Ind Eng Chem* 43:61–68
- Bediako JK, Wei W, Yun Y-S (2016c) Low-cost renewable adsorbent developed from waste textile fabric and its application to heavy metal adsorption. *J Taiwan Inst Chem Eng* 63:250–258
- Bediako JK, Reddy DHK, Song M-H, Wei W, Lin S, Yun Y-S (2017) Preparation, characterization and lead adsorption study of triphosphosphate-modified waste Lyocell fibers. *J. Env. Chem. Eng.* 5:412–421
- Bediako JK, Park SW, Choi J-W, Song M-H, Yun Y-S (2019a) High-performance and acid-tolerant polyethylenimine-aminated polyvinyl chloride fibers: fabrication and application for recovery of platinum from acidic wastewaters. *J. Environ. Chem. Eng.* 7:102839
- Bediako JK, Sarkar AK, Lin S, Zhao Y, Song M-H, Choi J-W, Cho C-W, Yun Y-S (2019b) Characterization of the residual biochemical components of sequentially extracted banana peel biomasses and their environmental remediation applications. *Waste Manag* 89:141–153
- Bedin KC, Martins AC, Cazetta AL, Pezoti O, Almeida VC (2016) KOH-activated carbon prepared from sucrose spherical carbon: adsorption equilibrium, kinetic and thermodynamic studies for methylene blue removal. *Chem Eng J* 286:476–484
- Bhattacharya AK, Venkobachar C (1984) Removal of cadmium (II) by low cost adsorbents. *J Environ Eng* 110:110–122
- Boparai HK, Joseph M, O'Carroll DM (2011) Kinetics and thermodynamics of cadmium ion removal by adsorption onto nano zerovalent iron particles. *J. Hazard. Mater.* 186:458–465
- Chen S, Zhang J, Zhang C, Yue Q, Li Y, Li C (2010a) Equilibrium and kinetic studies of methyl orange and methyl violet adsorption on activated carbon derived from *Phragmites australis*. *Desalination* 252:149–156
- Chen W, Zhang H, Huang Y, Wang W (2010b) A fish scale based hierarchical lamellar porous carbon material obtained using a natural template for high performance electrochemical capacitors. *J Mater Chem* 20:4773–4775
- Dada AO, Olalekan AP, Olatunya AM, Dada O (2012) Langmuir, Freundlich, Temkin and Dubinin-Radushkevich isotherms studies of equilibrium sorption of Zn^{2+} onto phosphoric acid modified rice husk. *IOSR J. Appl. Chem.* 338–345
- Dambies L, Guimon C, Yiacoumi S, Guibal E (2001) Characterization of metal ion interactions with chitosan by X-ray photoelectron spectroscopy. *Colloids Surf A Physicochem Eng Asp* 177:203–214
- de Paiva TMN, Fraga TJM, Sales DCS, Carvalho MN, da Motta Sobrinho MA (2018) Anomalocardia brasiliana shellfish shells as a novel and ecofriendly adsorbent of Nylosan Brilliant Blue acid dye. *Water Sci Technol* 78:1576–1586
- Dementjev AP, de Graaf A, Naumkin AV, van de Sanden MCM, Serov AA (2000) X-ray photoelectron spectroscopy reference data for identification of the C_3N_4 phase in carbon-nitrogen films. *Diam Relat Mater* 9:1904–1907
- Deng H, Lu J, Li G, Zhang G, Wang X (2011) Adsorption of methylene blue on adsorbent materials produced from cotton stalk. *Chem Eng J* 172:326–334
- Oliveira EHCD, Marques Fraga DMS, da Silva MP, TJM F, Carvalho MN, de Luna Freire EMP, Ghislandi MG, da Motta Sobrinho MA

- (2019) Removal of toxic dyes from aqueous solution by adsorption onto highly recyclable xGnP® graphite nanoplatelets. *J Environ Chem Eng* 7
- Foo KY, Hameed BH (2012) Preparation, characterization and evaluation of adsorptive properties of orange peel based activated carbon via microwave induced K_2CO_3 activation. *Bioresour Technol* 104:679–686
- Fraga TJM, dos Santos Marques Fraga DM, da Silva TC, Carvalho MN, da Motta Sobrinho MA (2018) Adsorption of reactive dyes onto thermally treated waste from aluminum lamination. *Water Prac Technol* 13:629–641
- Freundlich HMF (1906) Über die Adsorption in Lösungen. *Z Phys Chem A*:385–470
- Girods P, Dufour A, Fierro V, Rogaume Y, Rogaume C, Zoulalian A, Celzard A (2009) Activated carbons prepared from wood particle-board wastes: characterisation and phenol adsorption capacities. *J Hazard Mater* 166:491–501
- González-Montelongo R, Gloria Lobo M, González M (2010) Antioxidant activity in banana peel extracts: testing extraction conditions and related bioactive compounds. *Food Chem* 119:1030–1039
- Ho Y-S (2006) Review of second-order models for adsorption systems. *J Hazard Mater* 136:681–689
- Ho Y-S, McKay G (1999) Pseudo-second order model for sorption processes. *Process Biochem* 34:451–465
- Huang W, Zhang H, Huang Y, Wang W, Wei S (2011) Hierarchical porous carbon obtained from animal bone and evaluation in electric double-layer capacitors. *Carbon* 49:838–843
- Jiang X, Xiang X, Peng S, Hou L (2019) Facile preparation of nitrogen-doped activated mesoporous carbon aerogel from chitosan for methyl orange adsorption from aqueous solution. *Cellulose* 26:4515–4527
- Kelm MAP, da Silva Junior MJ, de Barros Holanda SH, de Araujo CMB, de Assis Filho RB, Freitas EJ, Dos Santos DR, da Motta Sobrinho MA (2019) Removal of azo dye from water via adsorption on biochar produced by the gasification of wood wastes. *Environ Sci Pollut Res Int* 26:28558–28573. <https://doi.org/10.1007/s11356-018-3833-x>
- Khaled A, El Nemr A, El-Sikaily A, Abdelwahab O (2009) Removal of Direct N Blue-106 from artificial textile dye effluent using activated carbon from orange peel: adsorption isotherm and kinetic studies. *J Hazard Mater* 165:100–110
- Kim MH, Hwang C-H, Kang SB, Kim S, Park SW, Yun Y-S, Won SW (2015) Removal of hydrolyzed Reactive Black 5 from aqueous solution using a polyethylenimine–polyvinyl chloride composite fiber. *Chem Eng J* 280:18–25
- Lagerge S, Zajac J, Partyka S, Groszek AJ (1999) Comparative study on the adsorption of cyanide gold complexes onto different carbonaceous samples: measurement of the reversibility of the process and assessment of the active surface inferred by flow microcalorimetry. *Langmuir* 15:4803–4811
- Langmuir I (1918) The adsorption of gases on plane surfaces of glass, mica and platinum. *J Am Chem Soc* 40:1361–1403
- Li Y, Du Q, Liu T, Sun J, Wang Y, Wu S, Wang Z, Xia Y, Xia L (2013) Methylene blue adsorption on graphene oxide/calcium alginate composites. *Carbohydr Polym* 95:501–507
- Li Y, Sun J, Du Q, Zhang L, Yang X, Wu S, Xia Y, Wang Z, Xia L, Cao A (2014) Mechanical and dye adsorption properties of graphene oxide/chitosan composite fibers prepared by wet spinning. *Carbohydr Polym* 102:755–761
- Liang S, Guo X, Feng N, Tian Q (2009) Application of orange peel xanthate for the adsorption of Pb^{2+} from aqueous solutions. *J Hazard Mater* 170:425–429
- Liu YT, Zhu XD, Duan ZQ, Xie XM (2013) Flexible and robust MoS_2 -graphene hybrid paper cross-linked by a polymer ligand: a high-performance anode material for thin film lithium-ion batteries. *Chem. Commun. (Camb)* 49:10305–10307
- Liu Z, Zhan X, Yang M, Yang Q, Xu X, Lan F, Wu Y, Gu Z (2016) A magnetic-dependent protein corona of tailor-made superparamagnetic iron oxides alters their biological behaviors. *Nanoscale* 8:7544–7555
- Mahmoudi K, Hosni K, Hamdi N, Srasra E (2014) Kinetics and equilibrium studies on removal of methylene blue and methyl orange by adsorption onto activated carbon prepared from date pits—a comparative study. *Korean J Chem Eng* 32:274–283
- Memon JR, Memon SQ, Bhangar MI, Memon GZ, El-Turki A, Allen GC (2008) Characterization of banana peel by scanning electron microscopy and FT-IR spectroscopy and its use for cadmium removal. *Colloid Surface B* 66:260–265
- Mokhtari P, Ghaedi M, Dashtian K, Rahimi MR, Purkait MK (2016) Removal of methyl orange by copper sulfide nanoparticles loaded activated carbon: kinetic and isotherm investigation. *J Mol Liq* 219:299–305
- Moreno-Castilla C (2004) Adsorption of organic molecules from aqueous solutions on carbon materials. *Carbon* 42:83–94
- Nekouei F, Kargarzadeh H, Nekouei S, Tyagi I, Agarwal S, Kumar Gupta V (2016) Preparation of nickel hydroxide nanoplates modified activated carbon for malachite green removal from solutions: kinetic, thermodynamic, isotherm and antibacterial studies. *Process Saf Environ Prot* 102:85–97
- Nethaji S, Sivasamy A, Mandal AB (2013) Adsorption isotherms, kinetics and mechanism for the adsorption of cationic and anionic dyes onto carbonaceous particles prepared from *Juglans regia* shell biomass. *Int J Environ Sci Technol* 10:231–242
- Ngulube T, Gumbo JR, Masindi V, Maity A (2017) An update on synthetic dyes adsorption onto clay based minerals: a state-of-art review. *J Environ Manag* 191:35–57
- Ofomaja AE (2007) Kinetics and mechanism of methylene blue sorption onto palm kernel fibre. *Process Biochem* 42:16–24
- Park SW, Bediako JK, Song M-H, Choi J-W, Lee H-C, Yun Y-S (2018) Facile fabrication of polyacrylic acid-polyvinyl chloride composite adsorbents for the treatment of cadmium-contaminated wastewater. *J Env Chem Eng* 6:2401–2408
- Patel M, Feng W, Savaram K, Khoshi MR, Huang R, Sun J, Rabie E, Flach C, Mendelsohn R, Garfunkel E, He H (2015) Microwave enabled one-pot, one-step fabrication and nitrogen doping of holey graphene oxide for catalytic applications. *Small* 11:3358–3368
- Pessôa TS, LED LF, da Silva MP, Pereira Neto LM, BFD N, TJM F, Jaguaribe EF, Cavalcanti JV, da Motta Sobrinho MA (2019) Açai waste benefiting by gasification process and its employment in the treatment of synthetic and raw textile wastewater. *J Clean Prod* 240
- Pezoti O, Cazetta AL, Souza IPAF, Bedin KC, Martins AC, Silva TL, Almeida VC (2014) Adsorption studies of methylene blue onto $ZnCl_2$ -activated carbon produced from buriti shells (*Mauritia flexuosa* L.). *J Ind Eng Chem* 20:4401–4407
- Pillai SS, Deepa B, Abraham E, Giriya N, Geetha P, Jacob L, Koshy M (2013) Biosorption of Cd(II) from aqueous solution using xanthated nano banana cellulose: equilibrium and kinetic studies. *Ecotoxicol Environ Safe* 98:352–360
- Qi X, Li L, Tan T, Chen W, Smith RL (2013) Adsorption of 1-butyl-3-methylimidazolium chloride ionic liquid by functional carbon microspheres from hydrothermal carbonization of cellulose. *Environ Sci Technol* 47:2792–2798
- Salima A, Benaouda B, Noureddine B, Duclaux L (2013) Application of *Ulva lactuca* and *Systoceira stricta* algae-based activated carbons to hazardous cationic dyes removal from industrial effluents. *Water Res* 47:3375–3388
- Sarkar AK, Saha A, Panda AB, Pal S (2015) pH triggered superior selective adsorption and separation of both cationic and anionic dyes and photocatalytic activity on a fully exfoliated titanate layer-natural polymer based nanocomposite. *Chem Commun (Camb)* 51:16057–16060

- Sarkar AK, Saha A, Tarafder A, Panda AB, Pal S (2016) Efficient removal of toxic dyes via simultaneous adsorption and solar light driven photodegradation using recyclable functionalized amylopectin-TiO₂-Au nanocomposite. *ACS Sust Chem Eng* 4:1679–1688
- Sarkar AK, Bediako JK, Choi J-W, Yun Y-S (2019): Functionalized magnetic biopolymeric graphene oxide with outstanding performance in water purification *NPG Asia Materials* 11
- Sharma YC, Uma SASK, Upadhyay SN (2010) Characterization and adsorption studies of *Cocos nucifera* L. activated carbon for the removal of methylene blue from aqueous solutions. *J Chem Eng Data* 55:2662–2667
- Song M, Duan Z, Qin R, Xu X, Liu S, Song S, Zhang M, Li Y, Shi J (2019) Simultaneous adsorption of Cd²⁺ and methylene blue from aqueous solution using xanthate-modified baker's yeast. *Korean J Chem Eng* 36:869–879
- Spreen TH (2010) Projections of world production and consumption of citrus to 2010. FAO Corporate Document Repository, Economic and Social Development Department. <http://www.fao.org/DOCREP/003/X6732E/x6732e_02.htm>
- Squarcialupi MC, Bernardini GP, Atrei A, Rovida G (2002) Characterisation by XPS of the corrosion patina formed on bronze surfaces. *J Cult Herit* 3:199–204
- Sun G, Li X, Qu Y, Wang X, Yan H, Zhang Y (2008) Preparation and characterization of graphite nanosheets from detonation technique. *Mater Lett* 62:703–706
- Tan IAW, Ahmad AL, Hameed BH (2008) Preparation of activated carbon from coconut husk: optimization study on removal of 2,4,6-trichlorophenol using response surface methodology. *J Hazard Mater* 153:709–717
- Tang J, Li Y, Wang X, Daroch M (2017) Effective adsorption of aqueous Pb²⁺ by dried biomass of *Landoltia punctata* and *Spirodela polyrhiza*. *J Clean Prod* 145:25–34
- Tran HN, You SJ, Hosseini-Bandegharai A, Chao HP (2017) Mistakes and inconsistencies regarding adsorption of contaminants from aqueous solutions: a critical review. *Water Res* 120:88–116
- Vargas AMM, Cazetta AL, Kunita MH, Silva TL, Almeida VC (2011) Adsorption of methylene blue on activated carbon produced from flamboyant pods (*Delonix regia*): study of adsorption isotherms and kinetic models. *Chem Eng J* 168:722–730
- Vijayaraghavan K, Yun YS (2007) Chemical modification and immobilization of *Corynebacterium glutamicum* for biosorption of reactive black 5 from aqueous solution. *Ind Eng Chem Res* 46:608–617
- Wagner CD (1979) Handbook of X-ray photoelectron spectroscopy: a reference book of standard data for use in X-ray photoelectron spectroscopy. Physical Electronics Division, Perkin-Elmer Corp
- Wang J, Kaskel S (2012) KOH activation of carbon-based materials for energy storage. *J Mater Chem* 22:23710–23725
- Wang X, Liu X, Yuan H, Liu H, Liu C, Li T, Yan C, Yan X, Shen C, Guo Z (2018) Non-covalently functionalized graphene strengthened poly(vinyl alcohol). *Mater Des* 139:372–379
- Won SW, Kim S, Kotte P, Lim A, Yun Y-S (2013): Cationic polymer-immobilized polysulfone-based fibers as high performance sorbents for Pt(IV) recovery from acidic solutions. *J. Hazard. Mater.* 263, Part 2, 391–397
- Xu T, He Y, Qin Y, Zhao C, Peng C, Hu J, Liu H (2018) Facile preparation of porous organic copolymer based on triptycene and crown ether for efficient organic dye adsorption. *RSC Adv* 8:4963–4968
- Yagci NU 2004: Production and characterisation of activated carbon from Apricot Stones, Middle East Technical University (METU), Ankara pages 19–105 pp
- Yagub MT, Sen TK, Afroz S, Ang HM (2014) Dye and its removal from aqueous solution by adsorption: a review. *Adv Colloid Interf Sci* 209:172–184
- Yahya MA, Al-Qodah Z, Ngah CWZ (2015) Agricultural bio-waste materials as potential sustainable precursors used for activated carbon production: a review. *Renew Sust Energ Rev* 46:218–235
- Yao Y, Bing H, Feifei X, Xiaofeng C (2011) Equilibrium and kinetic studies of methyl orange adsorption on multiwalled carbon nanotubes. *Chem Eng J* 170:82–89
- Zequine C, Ranaweera CK, Wang Z, Dvornic PR, Kahol PK, Singh S, Tripathi P, Srivastava ON, Singh S, Gupta BK, Gupta G, Gupta RK (2017) High-performance flexible supercapacitors obtained via recycled jute: bio-waste to energy storage approach. *Sci Rep* 7:1174
- Zhang Z, Zhang Z, Fernández Y, Menéndez JA, Niu H, Peng J, Zhang L, Guo S (2010) Adsorption isotherms and kinetics of methylene blue on a low-cost adsorbent recovered from a spent catalyst of vinyl acetate synthesis. *Appl Surf Sci* 256:2569–2576
- Zhou D, Zhang L, Guo S (2005) Mechanisms of lead biosorption on cellulose/chitin beads. *Water Res* 39:3755–3762

Publisher's note Springer Nature remains neutral with regard to jurisdictional claims in published maps and institutional affiliations.